Description and Caveats for the LAT Team Model of Diffuse Gamma-Ray Emission
Version: gll_iem_v02.fit

Diffuse and Molecular Clouds Science Working Group
Fermi Large Area Telescope Collaboration

August 24, 2009

1 Principle

The high-energy Galactic γ-ray emission is produced by the interaction of energetic cosmic-ray electrons and protons with interstellar nucleons and photons. The decay of neutral pions produced in hadron collisions, the inverse Compton scattering of the interstellar radiation field (ISRF) by electrons and their bremsstrahlung emission in the interstellar medium (ISM) are the main contributors to the Galactic emission.

Underlying our modeling efforts is that energetic cosmic rays uniformly penetrate all gas phases in the ISM. Then the diffuse γ-ray intensity in each direction can be modeled as a linear combination of gas column-densities, an inverse Compton intensity map (I_{IC}), and an isotropic intensity (I_{iso}) that accounts for the extragalactic background and the residual instrumental background.

About 99% of the mass of the ISM is gas, and about 90% of this gas is atomic (H I) or molecular hydrogen (H_2). H I is traced by its radio 21-cm line radiation, but H_2 without any permanent dipole can not reliably be observed directly in its dominantly cold phase. The observation of molecular gas relies on other molecules and especially on the 2.6-mm line of carbon monoxide (CO). The rotationally excited state of CO is caused by collision with H_2 molecules, so the radio emission of CO can trace H_2. As has been usual in studies of diffuse gamma-ray emission, the column densities N(H I) are derived from the 21-cm line temperatures on the assumption of a uniform spin temperature and $N(H_2)$ column-densities are assumed to be proportional to the line intensities W(CO).

Reddening E(B-V) maps trace the total dust column-densities. Away from photodissociation regions and hot star-forming regions where dust infrared emissivities can vary dramatically, cold dust is supposed to be well mixed with the gas and thus provides a good template for the total gas. The residual reddening map E(B-V)$_{res}$, obtained after subtracting the part linearly correlated with the N(H I) column-densities and W(CO) intensities, has been used in the model as a gas column-density "correction".

To allow for a Galactocentric gradient of cosmic-ray flux in the Galaxy, the N(H I) column-densities and W(CO) intensities have been derived for six Galactocentric rings (see section 3). For a given energy band the predicted count rate is therefore calculated as:

$$N_{pred}(l,b) = \iint d\Omega_k \left(\sum_{i=rings} [q_{HI,i} N_{HI}(r_i, l_k, b_k) + q_{CO,i} W_{CO}(r_i, l_k, b_k)] \right.$$
$$\left. + q_{EBV} E(B-V)_{res}(l_k, b_k) + q_{IC} I_{IC}(l_k, b_k) + I_{iso}(l_k, b_k) \right) \epsilon(l_k, b_k)\, PSF(l, b, l_k, b_k)$$
$$+ \sum_{j=sources} F_j\, \epsilon(l_j, b_j)\, PSF(l_j, b_j, l, b)$$

$$(1)$$

Here $\epsilon(l,b)$ represents the exposure of the LAT as a function of Galactic coordinates and F_j notes point-source fluxes. PSF denotes a 2-dimensional projection of the point-spread function for the energy range under consideration. We fit this model to the LAT data to determine the emissivities (q) of the Galactic diffuse components as well as the isotropic background (I_{iso}). The point sources included in the model were taken from an analysis of the first 9 months of LAT science data, using a preliminary model of the diffuse emission. The positions and fluxes of the sources were not refit in this analysis. The LAT has a large field of view and effective area; with the data accumulated since the start of the science phase of the mission we were able to perform a fit in ten energy bands, logarithmically distributed between 100 MeV and 10 GeV, and from these to determine the differential emissivities $\frac{dq}{dE}$ for all the components and $I_{iso}(E)$.

For the fitting we have used a 2-dimensional binned maximum-likelihood method with Poisson statistics using maps in 0.5 x 0.5 degree bins. The likelihood (L) is calculated as the product, for all the pixels, of the Poisson probabilities of observing $N_{obs}(l,b)$ photons in a pixel where the model predicts $N_{pred}(l,b)$. As a first step, the fit in the 10 independent energy bands has been used to determine the spectral shapes of the emissivities. These were then frozen and, in a second step, their relative normalization was ob-

tained by fitting the single band gamma-ray map integrated from 0.3 to 20 GeV. This step made use of the better point-spread function (PSF) and very large statistics to allow a better spatial separation of the components. The boundaries of the six rings were chosen to maximize the spatial differences between the maps, but there is still significant degeneracy between them near the plane toward the inner Galaxy at the level of the LAT resolution. The final fit has therefore been performed in ordered steps, freezing the relevant parameters after each step: first at $|b| > 5°$ to get the ring that spans the solar circle and the large-scale reddening and inverse Compton, then at $|l| > 90°$ and all latitudes for the outer rings, and over the whole sky to obtain the inner rings and isotropic components. Knowledge of the gas distribution and CR variations in the Galactic plane is lacking and this method minimizes the effects of the bright Galactic ridge on high latitude Galactic diffuse emission.

The following sections detail the data used and the resulting models for the Galactic diffuse emission and the isotropic background. Caveats for their use are also provided.

2 Data Selection

For this study we have used diffuse-class events recorded between August 2 2008 and May 29 2009 (r0239399889 to r0265244776), which is close to 10 months of LAT science data. The exposure and PSF files maps were generated using the P6_V3_DIFFUSE instrument response function. Photon maps were binned in HEALPix format with the *Gardian* analysis tool developed by the LAT team (see [Ackermann et al., 2008]), with a maximum zenith angle of 105° to limit Earth albedo contamination. We also used *Gardian* to convolve each model component with the LAT PSF in each of the ten energy bands and in the 0.3–20 GeV integrated bin using the observed spectrum to weight the energy-dependent PSF

3 Model Components

The all-sky Leiden-Argentina-Bonn (LAB) ([Kalberla et al., 2005]) composite survey was used to obtain the atomic hydrogen N(H I) column densities on the assumption of a uniform spin temperature of 200 K. Regions of strong H I absorption against bright continuum sources were interpolated across. Nearby galaxies LMC, SMC, and M31 that were within the velocity range of the LAB survey were excised. They are well separated in velocity from the

Milky Way. The velocity integrated CO intensities $W(CO)$ were obtained from the Center for Astrophysics compilation ([Dame et al., 2001]) as well as new dedicated observations obtained at mid-latitudes, up to $|b| = 30°$ in the northern, with the same telescope. The integrated intensities were derived using 'moment mask' filtering to enhance the signal-to-noise ratios, in particular along the faint cloud edges and for tiny clumps off the plane. In our study, we did not assume any value for the H_2-to-CO conversion factor; on the contrary, we obtained it from the fit.

We used the reddening E(B-V) map of [Schlegel et al., 1998]. Most of the reddening is well correlated with the N(H I) column-densities and W(CO) intensities. Subtracting the correlated parts from the total reddening reveals coherent structures or "clouds" across the sky with small negative residuals (-0.2 to 0 magnitude, typically) and other clouds with more pronounced positive residuals (0 to 0.6 mag). The former are related to the light and diffuse cirruses in which an average H I spin temperature of 200 K is likely to be too low (thus N(H I) is overestimated). The latter reveal gas in addition to that traced by N(H I) and W(CO). It resides predominantly at the interface between the H I and CO structures [Grenier et al., 2005]. This gas can be cold dense H I not accounted for in the N(H I) maps in regions where the spin temperature is closer to 30 or 40 K [Heiles & Troland, 2003]. It is also likely to be moderately dense H_2 that is known to exist in abundance at the interface between the atomic and molecular phases, but that is not dense enough ($< 10^3$ cm^{-3}) to efficiently excite CO lines, typically for E(B-V) < 0.6 ([Lombardi et al., 2006, Leroy et al., 2009]). Infrared point sources present in the reddening map have been filtered out before use.

Maps of $N(H I)$ and $W(CO)$ were derived in 6 galactocentric rings using the rotation curve of Clemens (1985), with the following limits (in kpc):

rings	r_{min}	r_{max}
1	0.0	4.0
2	4.0	5.5
3	5.5	7.0
4	7.0	10.0
5	10.0	16.5
6	16.5	50.0

While the different gas column-density maps offer a template for photons originating from π^0-decay and Bremsstrahlung emission, there is no simple template for the inverse-Compton emission I_{IC}. Instead this must be calculated and we use the prediction from the GALPROP [1] code with galdef

---

[1]http://galprop.stanford.edu

identification prefix 54_77 for its spatial distribution. The ISRF used in the calculation is described in [Porter et al., 2008] (the maximal metallicity gradient model). The GALPROP code is run to obtain the primary and secondary cosmic-ray electron and positron intensities and spectra throughout the Galaxy. The calculation takes into account propagation and all energy losses and gains, with the IC energy losses for the cosmic-ray electrons and positrons (including Klein-Nishina effects) calculated using the full spatial and energy distribution of the ISRF. The propagated cosmic-ray electron and positron intensities and spectra are folded with the ISRF to obtain the IC emissivity throughout the Galaxy, and these are integrated along the line-of-sight for each direction to obtain the IC intensity skymaps.

Based on the finding of small, but systematic and large-scale residuals with this model, we added to the model local structures in the diffuse emission not accounted for by the all-sky gas rings and dust maps, including local radio structures and free q_{CO} emissivity for regions around Cygnus and Aquila Rift.

4   Results from the fit

We have fitted each component of Eq. 1 in the 10 energy bands. We obtained for each ring the emissivity spectrum, as well as renormalization coefficients for the inverse Compton and an isotropic component. The former is expected to be near 1, i.e., no major modifications required for the inverse Compton intensity or spectrum, and that was the case. In order to validate the complete fitting method, we compared the emissivity results with predictions from GALPROP and with previous measurements. Their values as well as their variations with energy and Galactocentric distance are in the expected range. This study will be detailed in a coming publication. The observed and modelled count maps are shown in Fig. 1 and Fig. 2 for gamma rays with energies between 300 MeV and 20 GeV. The residual map found between the best fit and the data is presented in Fig. 3. It displays the statistical difference, $(N_{obs} - N_{pred})/\sqrt{N_{pred}}$, between the observed counts and those predicted from the diffuse background and bright sources using Eq. 1. The diffuse model itself, integrated over the same energy range and scaled by the exposure, is shown in Fig. 4 with the same scaling.
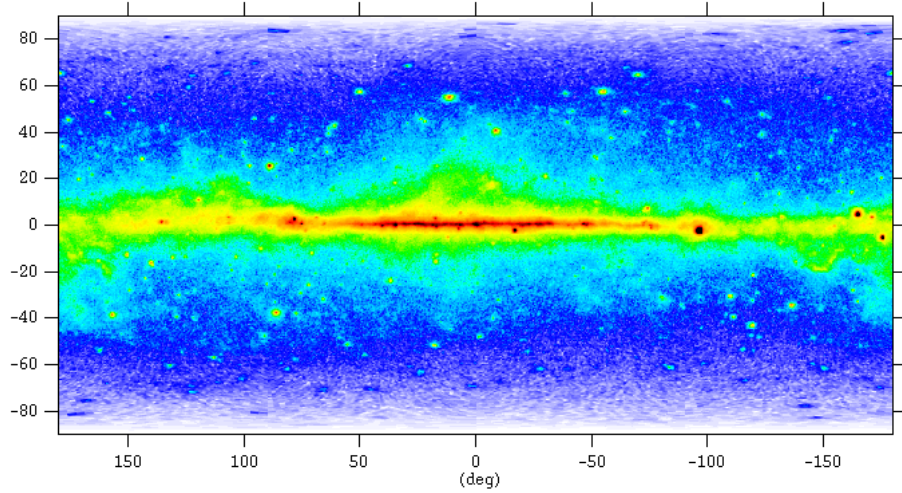
Figure 1: LAT all-sky γ-ray count map, $N_{obs}(l, b)$, in the 0.3–20 GeV energy band, in log-scale.
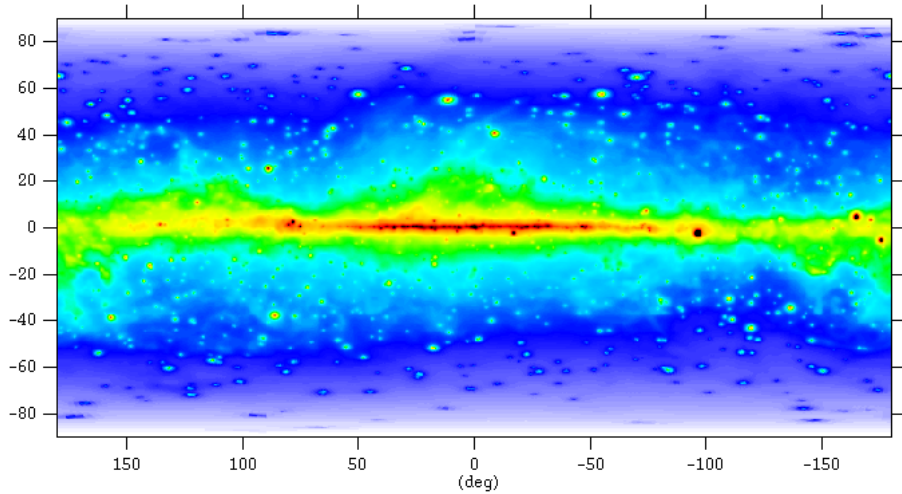
Figure 2: Diffuse model prediction *together with modeled point sources*, $N_{pred}(l, b)$, in the 0.3–20 GeV energy band. The photon counts are displayed with the same log-scale as in Fig. 1.

6
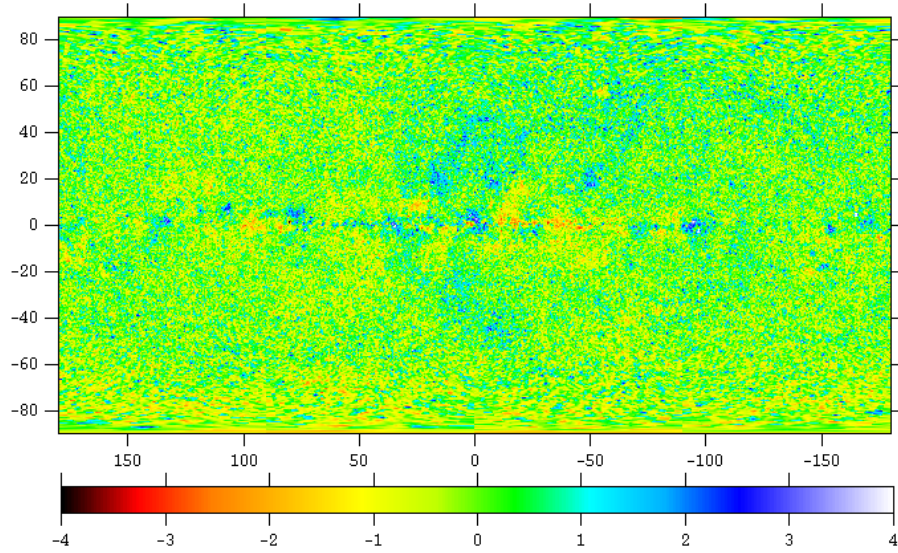
Figure 3: Residual map expressed in sigma values: $(N_{obs} - N_{pred})/\sqrt{N_{pred}}$
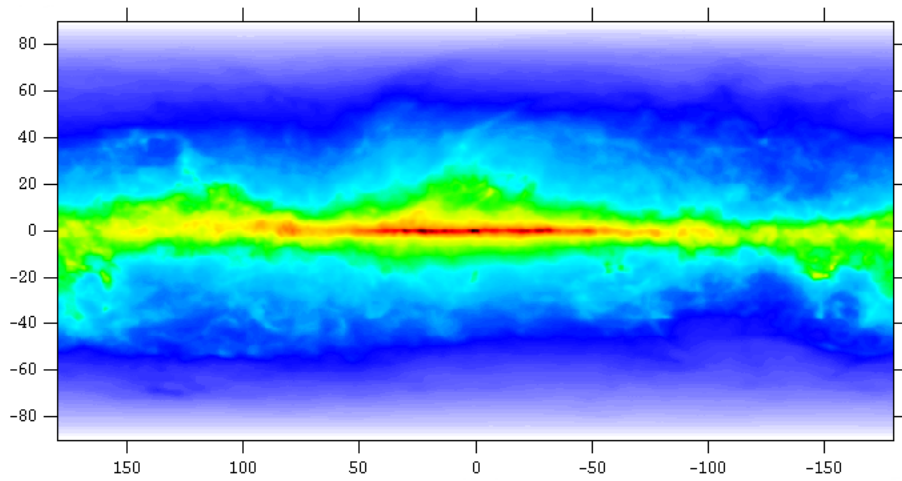
Figure 4: Diffuse model prediction alone, in the 0.3–20 GeV energy band. The photon counts are displayed with the same log-scale as in Figs. 1 and 2.

5 Resulting model of Galactic diffuse emission

Once we know the differential emissivity or normalization for each template, we can sum components to calculate the Galactic diffuse emission differential intensity in photons $\text{sr}^{-1} \text{ s}^{-1} \text{ cm}^{-2} \text{ MeV}^{-1}$:

$$
\begin{aligned}
\frac{dI}{dE}(l,b) &= \sum_{i=rings} \frac{dq_{HI,i}}{dE} N_{HI}(r_i,l,b) + \sum_{i=rings} \frac{dq_{CO,i}}{dE} W_{CO}(r_i,l,b) \\
&+ \frac{dq_{EBV}}{dE} E(B-V)_{res}(l,b) + \frac{dq_{IC}}{dE} I_{IC}(l,b)
\end{aligned}
\tag{2}
$$

For energies above 20 GeV the model has been extrapolated and globally renormalized to fit the LAT data so that the final model cube comprises 30 logarithmically-spaced energies between 50 MeV and 100 GeV. The model supplied in the $gll\_iem\_v02.fit$ FITS file gives the Galactic differential intensity in photons $\text{sr}^{-1} \text{ s}^{-1} \text{ cm}^{-2} \text{ MeV}^{-1}$. (The designation of the model is by prior agreement with the FSSC regarding the naming convention of LAT science data products. gll is for GLAST LAT, iem for interstellar emission model.) The isotropic component is not included in the cube, but is provided separately as a tabulated spectrum.

6 Model of isotropic emission

The isotropic component was determined separately from the Galactic diffuse component in a maximum likelihood fit including only high latitude emission ($|b| > 30°$). This was done to minimize the effects of the bright Galactic ridge that can be significant above $\sim 10°$ from the plane at low energies due to the long tails of the PSF. The spectrum of the isotropic emission including background is shown in Fig. 5 and tabulated in the $isotropic\_iem\_v02.txt$ file. It is continued to energies greater than 100 GeV using a simple extrapolation (linear in the logarithm of energy) of $gll\_iem\_v02.fit$.

Even though the isotropic component can be determined with great statistical accuracy, there are several systematic uncertainties that are difficult to determine precisely. First of all, the isotropic component includes any true extragalactic component as well as charged particle background misreconstructed as γ-rays. While both are believed to be rather homogeneous, there is no guarantee that their emissivity be precisely isotropic. For instance, if the extragalactic component consists of unresolved point sources, small anisotropies may result from the high variability of AGN and the latitude dependent sensitivity of the LAT instrument. Our current knowledge of the foreground Galactic emission is not precise enough to assess the
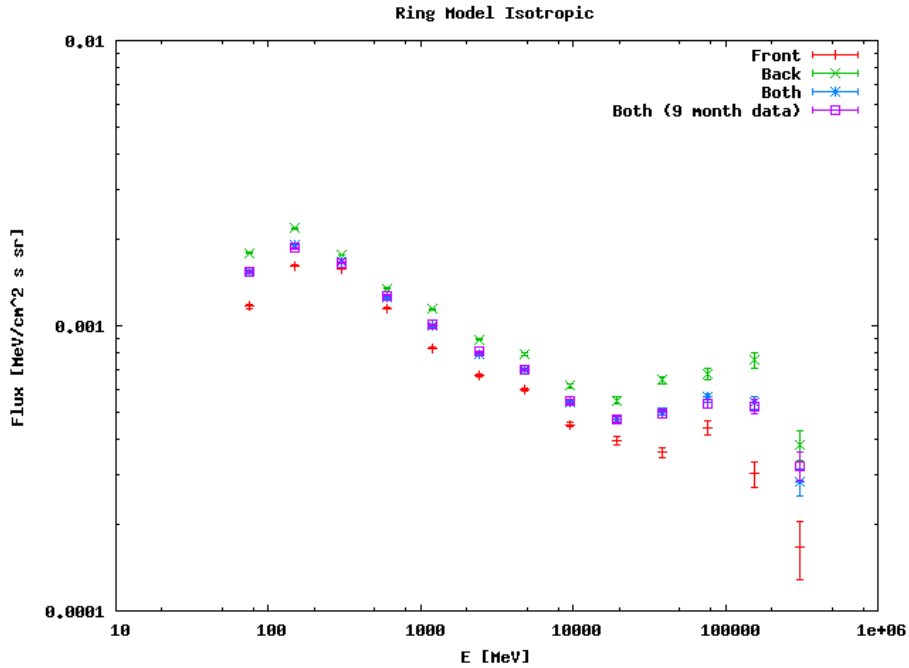
Figure 5: Isotropic spectrum for analysis of LAT data. Separate spectra are presented for Front and Back converting events because the residual charged-particle background is different for them, the contamination by residual background being greater in the Back section. The 'Both' spectrum is the overall average. These are valid *only* for the P6_V3_DIFFUSE response functions and the *gll_iem_v*02.*fit* model of Galactic diffuse emission. Note that what is plotted in each case is E^2 times the differential intensity. **The broad feature near 100 GeV is understood to be due to residual heavy cosmic rays in the Pass 6 analysis and is not astrophysical.**

anisotropies of the extragalactic background. In addition, the acceptance for residual charged-particle background is not the same as for gamma rays. That is, the distribution of arrival directions in instrument coordinates is not the same as for gamma rays and our modeling it as isotropic with the gamma-ray response functions is only an approximation.

7   Caveats

The model for the Galactic diffuse emission $gll\_iem\_v02.fit$ is the most accurate overall that the LAT team has produced. That the model is not perfect is evident in Fig. 3. Here are some salient cautions about the model and interpretation of the LAT observations in terms of the model.

• Especially at low latitudes residuals between the model and the LAT data are non-negligible and clumped. Well-known interstellar complexes deviate either positively (the model falls a little short of the data) or negatively. This is because they deviate from the average behaviour that has been inferred from the present fits, either because their cosmic-ray flux is slightly different, or because of non-linearities in the gas tracers and column-density derivations. The assumption of uniform spin temperature is not perfect, and at low latitudes in particular determinations $N(\text{H I})$ can be strongly affected by self absorption. These deviant structures are expected to have an effect on the detection and characterization of point sources. For instance, the "blue" hot spots of negative residuals in Orion, which are caused by the bright OB associations, have been checked to induce faint spurious gamma-ray sources. The clumpiness of the residuals for the current model of Galactic diffuse emission is a caution about using this model to search for extended sources at low latitudes.

• The model does not include populations of unresolved Galactic point sources, which may contribute of order 10% to the 'diffuse' emission. This is an additional reason for the deviations from the model, especially at low latitudes

• The absolute intensity level of the model for Galactic diffuse emission has low-level, large-scale deviations from the truth owing to approximations made in modeling the IC component. The IC emissivity calculation uses the Compton cross section averaged over incoming photon directions, that is, the target photon fields are assumed to have an isotropic angular distribution. This is true only for the cosmic microwave background. We have investigated the IC contribution using the anisotropic Compton cross section [Moskalenko & Strong, 2000] with the full angular distribution of the ISRF.

For the assumed ISRF, depending on direction the isotropic approximation can systematically underestimate the IC contribution by a factor of up to approximately 2. At high latitudes, the IC intensity can represent a large fraction of the Galactic diffuse emission. This effect has only been partially studied at this time due to the high computational cost of calculating the anisotropic IC skymaps. In addition, systematic uncertainties associated with the model of the ISRF itself are also being studied. Results will be reported in subsequent updates of the diffuse model.

• Within $10°$ of the Galactic center and anticenter, the radio and millimeter line surveys of H I and CO lose kinematic resolution and the distributions of the gas along the line of sight were interpolated from their distributions at longitudes just outside these ranges. The method, used for $|b| < 4°$ for CO and $|b| < 30°$ for H I, preserves the overall $W(\text{CO})$ and $N(\text{H I})$ but the systematic uncertainties in the diffuse gamma-ray intensities are necessarily larger in these regions. Their spatial distribution is also necessarily much flatter than in reality.

• The gas column-density correction derived from dust suffers from uncertain dust colour temperature corrections in the confused regions within a few degrees of the Galactic plane, especially near OB associations. The spatial resolution of the temperature correction map used by [Schlegel et al., 1998] is only $1.1°$ (FWHM).

• The diffuse model for energies below 120 MeV was not fitted to the data and is therefore less reliable.

• For energies above 50 GeV, the number of photons produced through interaction with the gas is probably underestimated compared to photons produced by IC scattering, so the spatial structure of the diffuse model above 50 GeV is probably too smooth.

• The diffuse model extends to 100 GeV in the current version, and the isotropic diffuse spectrum with residual background at higher energies was derived based on an extrapolation of that model. Studies of sources and diffuse emission at energies greater than 100 GeV are likely to be limited primarily by photon statistics but the reduced accuracy of the modeling at these energies should be kept in mind as well.

References

[Ackermann et al., 2008] Ackermann, M., et al. 2008, AIP Conf. Proc. No. 1085, (AIP, New York), p. 763

[Dame et al., 2001] Dame, T. M., Hartmann, D., & Thaddeus, P. 2001, ApJ, 547, 792

[Grenier et al., 2005] Grenier, I. A., Casandjian, J.-M., & Terrier, R. 2005, Science, 307, 1292

[Heiles & Troland, 2003] Heiles, C., & Troland, T. H. 2003, ApJ, 586, 1067

[Kalberla et al., 2005] Kalberla, P. M. W., Burton, W. B., Hartmann, D., Arnal, E. M., Bajaja, E., Morras, R., Pöppel, W. G. L. 2005, A&A, 440, 775

[Leroy et al., 2009] Leroy, A. K., et al., arXiv:0907.2240v1

[Lombardi et al., 2006] Lombardi, M., Alves, J., & Lada, C. J. 2006, A&A, 454, 781

[Moskalenko & Strong, 2000] Moskalenko, I. V. & Strong, A. W. 2000, ApJ 528, 357

[Porter et al., 2008] Porter, T. A., Moskalenko, I. V., Strong, A. W., Orlando, E., & Bouchet, L. 2008, ApJ, 682, 400

[Schlegel et al., 1998] Schlegel, D. J., Finkbeiner, D. P., & Davis, M. 1998, ApJ, 500, 525